Supplementary figures

Supplementary figure 1

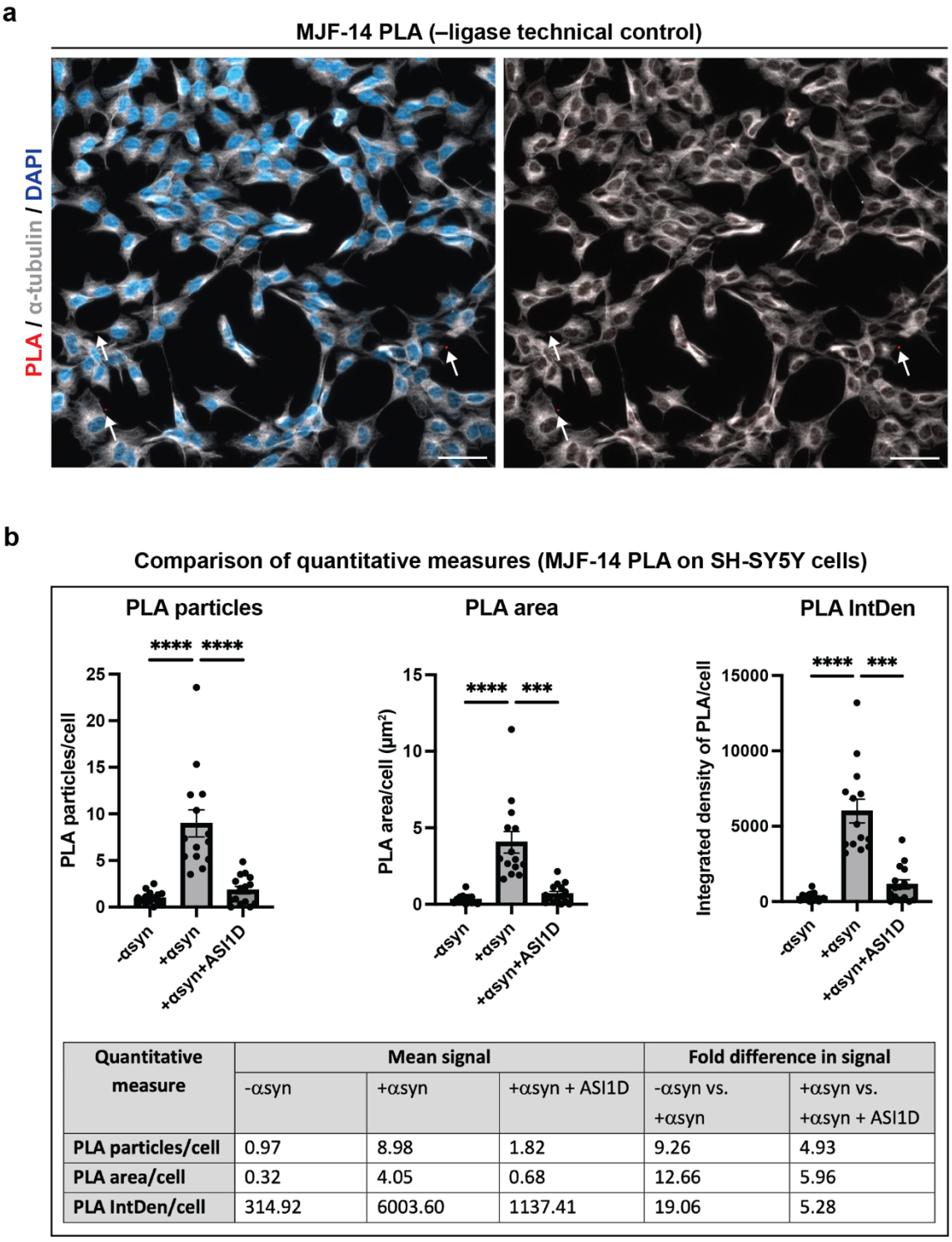

Quantitative measure	Mean signal			Fold difference in signal	
	-αsyn	+αsyn	+αsyn + ASI1D	-αsyn vs. +αsyn	+αsyn vs. +αsyn + ASI1D
PLA particles/cell	0.97	8.98	1.82	9.26	4.93
PLA area/cell	0.32	4.05	0.68	12.66	5.96
PLA IntDen/cell	314.92	6003.60	1137.41	19.06	5.28

Supplementary figure 1: Technical controls and additional quantification measures for MJF-14 PLA in SH-SY5Y cells.
a Technical negative PLA control without the ligase in the reaction mixture show virtually no PLA signal, confirming specificity of signal in the images presented in Fig. 1. Representative images of cultures immunostained with MJF-14 PLA (red), α-tubulin (grey), and DAPI nuclear stain (blue). Arrows indicate the rare signal in the red channel. Scale bars = 50 µm. **b** Comparison of various quantification measures in one set of cultures ± α-synuclein overexpression and ± ASI1D treatment. Increasing fold difference in signal (especially between -α-syn and +α-syn conditions) is seen when quantifying PLA area/cell or integrated density of PLA signal/cell compared to PLA particle counts/cell. Graphs display mean ± SEM from one replicate and each dot signifies one image. Experiments were performed minimum three times independently, and groups were compared using a Kruskal-Wallis one-way ANOVA followed by the Dunn post hoc test. *** p<0.001, **** p<0.0001.

Supplementary figure 2

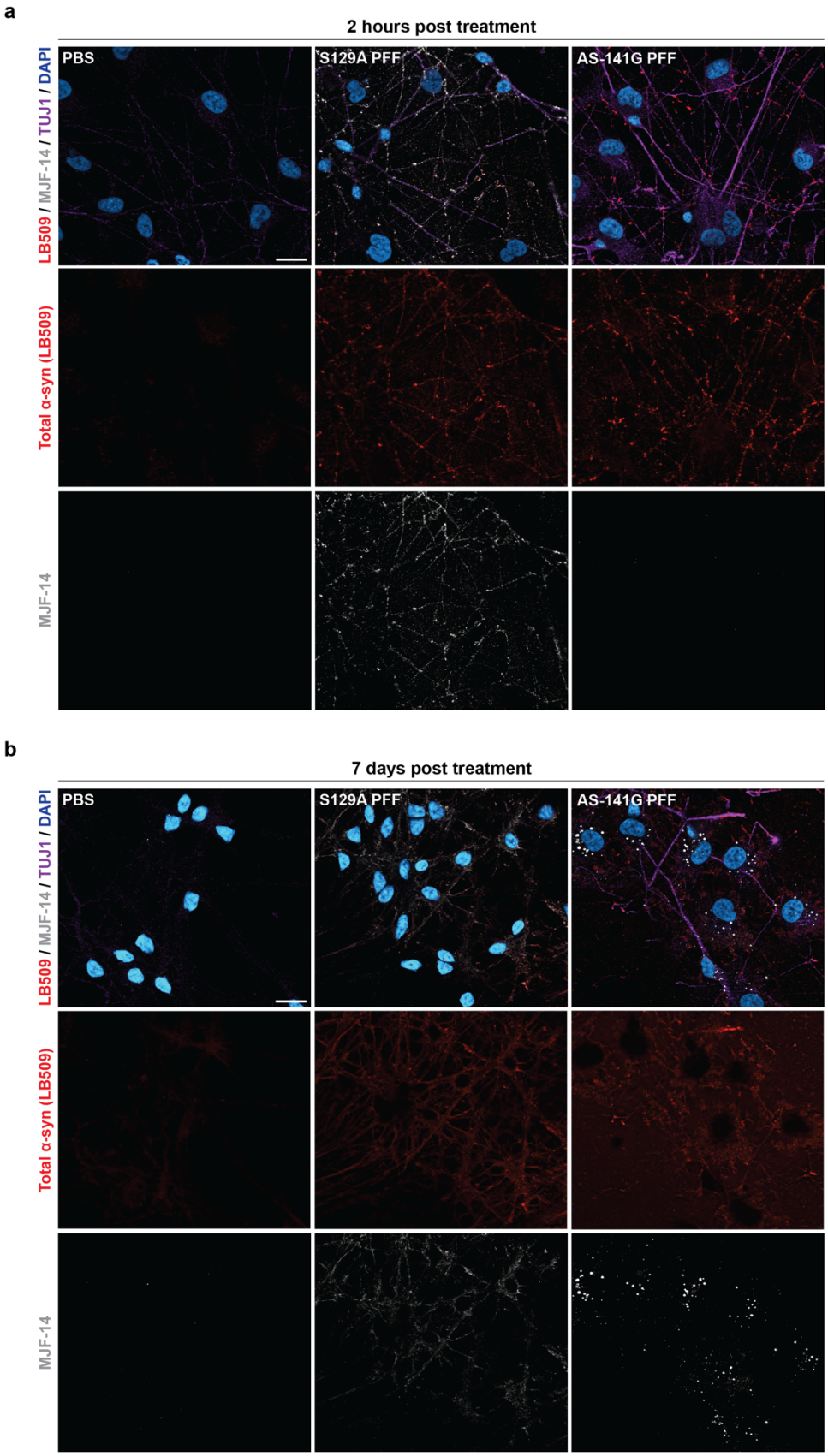

Supplementary figure 2: AS-141G PFFs are invisible to the MJF-14 antibody and increase signal-to-noise ratio in immunofluorescence staining of human cortical neurons.

a-b Immunofluorescence of human cortical neurons treated with either S129A PFFs, AS-141G PFFs, or PBS, and fixed after 2 hours (**a**) or 7 days (**b**). Representative images of cultures immunostained with MJF-14 (grey), total α-synuclein (LB509, red), βIII-tubulin (purple), and DAPI nuclear stain (blue) show strong detection of exogenous S129A PFFs with MJF-14 after 2 hours, while AS-141G PFFs don't generate any signal (**a**). After 7 days, increased MJF-14 staining is seen with both S129A and AS-141G PFF treatment, but considerable background staining, perhaps from non-internalized PFFs, is still present in S129A PFF cultures. In contrast, α-synuclein deposits in AS-141G PFF cultures are easily identifiable based on the MJF-14 staining (**b**). Scale bars = 20 µm.

Supplementary figure 3

a

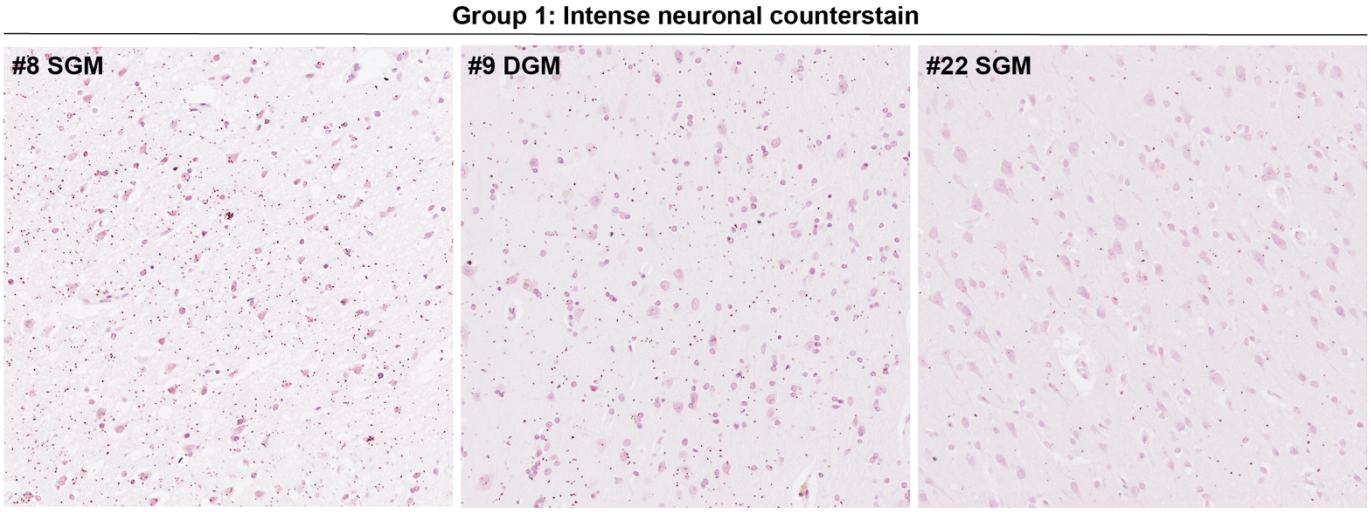

b

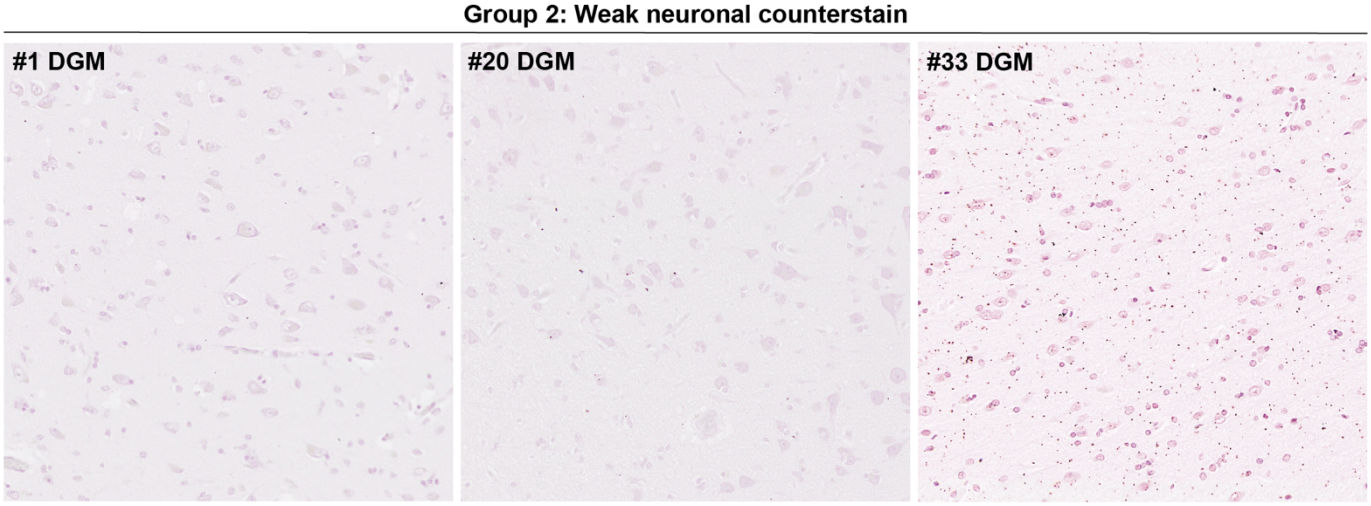

c

	Sensitivity	Precision	Accuracy
Definition	$\frac{true\ positive}{true\ positive\ +\ false\ negative}$	$\frac{true\ positive}{true\ positive\ +\ false\ positive}$	$\frac{true\ positive}{true\ positive\ +\ false\ positive + false\ negative}$

d

Group 1: Intense counterstain

	Sensitivity	Precision	Accuracy
#8 SGM	0.71	0.85	0.63
#9 DGM	0.91	0.69	0.65
#22 SGM	0.88	0.70	0.64
Mean	0.83	0.75	0.64

e

Group 2: Weak counterstain

	Sensitivity	Precision	Accuracy
#1 DGM	0.90	0.53	0.50
#20 DGM	0.98	0.68	0.67
#33 DGM	0.74	0.77	0.61
Mean	0.87	0.66	0.59

Supplementary figure 3: Optimization of automated segmentation of chromogenic PLA-stained human anterior cingulate cortex.

a-b ROIs used for optimization of PLA signal and nuclei segmentation grouped into either intense counterstain (**a**) or weak counterstain (**b**). Numbers indicate case ID, while SGM and DGM signify superficial and deep grey matter, respectively. The total number of PLA particles per image and classification into counterstain group for all cases can be found in Suppl. Table 1. **c** Definition of parameters for evaluation of segmentation classifier performance. **d-e** Final parameter values for intense (**d**) and weak (**e**) neuronal counterstain groups, respectively.

Supplementary figure 4

Strategy for image segmentation and analysis

1 Selection of test cohort for development of image classifier + manual annotation of test cohort

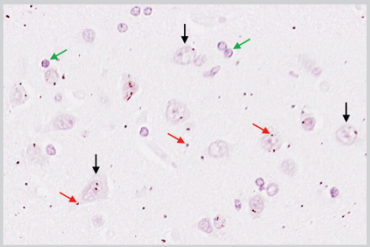

2 Training and validation of classifier

3 Get probability maps for nuclei and PLA signal

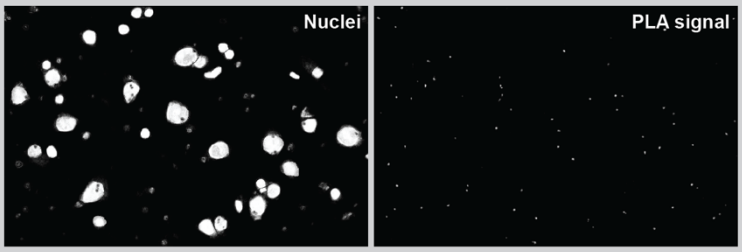

Add probability threshold
Filter on size (neurons >350 pixels)

Add probability threshold
Watershed to separate particles

4 Analyze total, neuronal and extra-cellular/glial areas, PLA dots and neuronal count

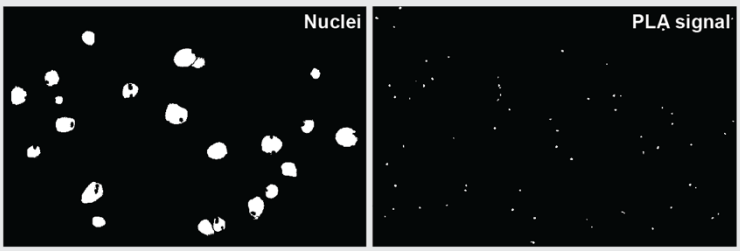

5 Analyze each neuron individually

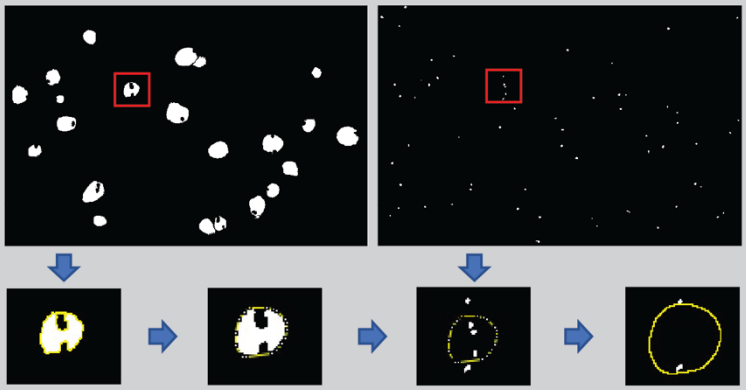

Select one neuronal nucleus

Fit convex hull (include indentations in nucleus)

Apply nuclear selection to PLA image, count dots and clear

Expand selection to include cytoplasm (3.5 µm border)

6 Group neurons according to table

No. of Neuron (Raw Counting data)								
Nuclear type		Cytoplasmic type		Mixed type				
1 PLA dot in nucleus + 0 PLA in cell body	>1 PLA dot in nucleus + 0 PLA in cell body	1 PLA dot in cell body + 0 PLA in nucleus	>1 PLA dot in cell body + 0 PLA in nucleus	1 PLA dot in nucleus + 1 PLA dot in cell body	>1 PLA dot in nucleus + 1 PLA dot in cell body	1 PLA dot in nucleus + >1 PLA dot in cell body	>1 PLA dot in nucleus + >1 PLA dot in cell body	No. of neurons without PLA signal

Supplementary figure 4: Strategy for image segmentation and quantification of PLA in human anterior cingulate cortex sections.
First, a test cohort consisting of 6 images was selected for the development and optimization of the automated classifier to segment the images (comprising differences in both PLA signal density and counterstain; see Suppl. Fig. 3). The test cohort was manually annotated before training of the classifier, which was then validated in its ability to correctly classify PLA signals and both glial and neuronal nuclei. For the classification of the entire ACC cohort, each image was then segmented and probability maps for nuclei and PLA signal were obtained. To define neuronal nuclei, a probability threshold was added, and particles larger than 350 pixels (36.7 µm^2, corresponding to an approx. diameter larger than 7 µm) were considered neuronal nuclei. To define PLA particles, a probability threshold was similarly added, fused particles separated using Watershed segmentation and particles with a size of 4-30 pixels (approx. 0.4-3.2 µm^2) counted. In addition, the total number of neuronal nuclei was counted, and total tissue area as well as glial/neuropil/extracellular area were computed, along with PLA particle counts in these compartments. For the single neuron analysis, each neuron was then analysed individually with 1) selection of nucleus, 2) fitting of a convex hull to include the indentations left by the PLA signal in the nuclei map, 3) application of the nuclear selection to the PLA signal map, counting of particles and clearing, and 4) expansion of nuclear selection by 3.5 µm to estimate cytoplasm, followed by counting of cytoplasmic PLA particles. Finally, each neuron was grouped in one of nine groups according to nuclear and cytoplasmic PLA particle counts.

Supplementary figure 5

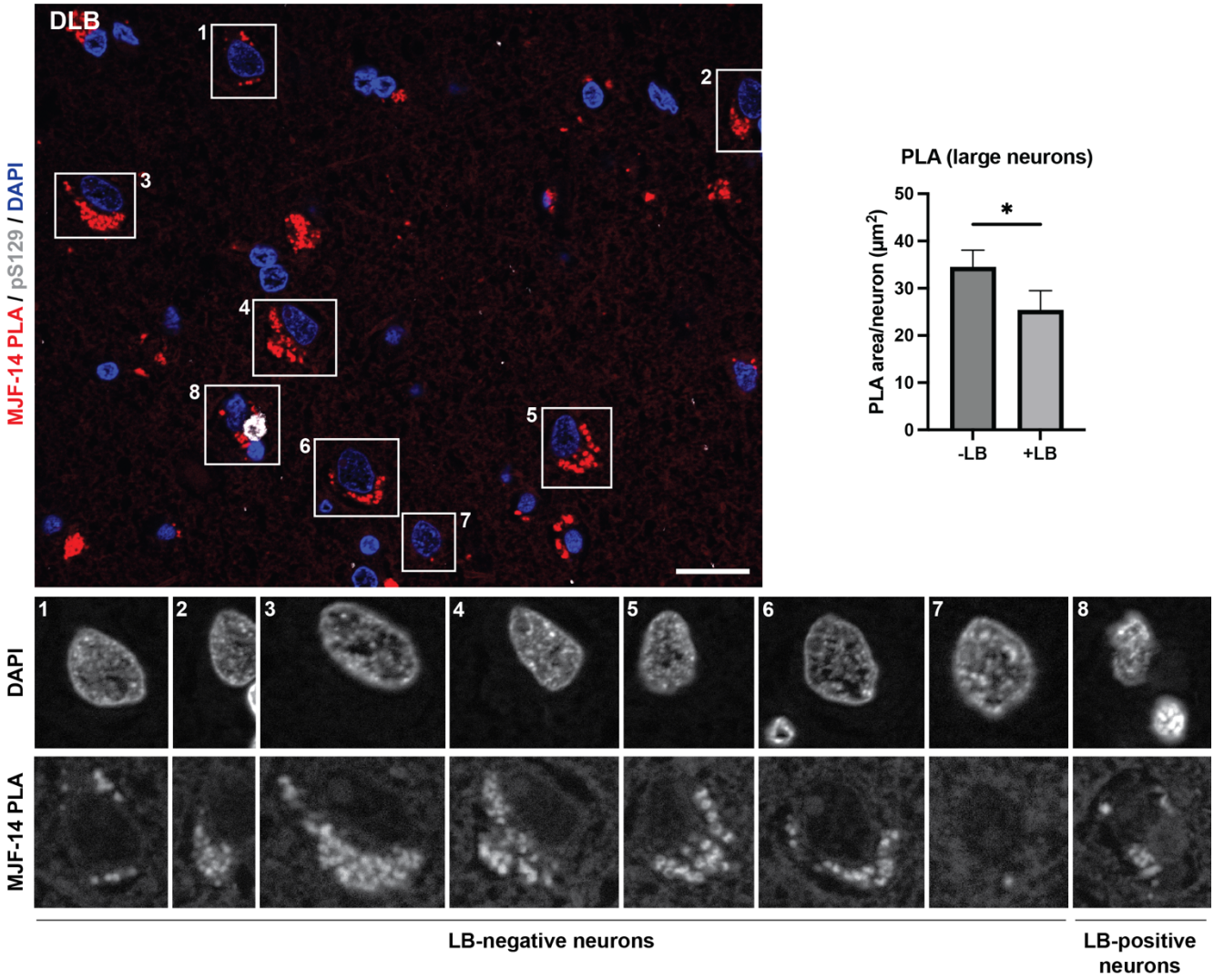

Supplementary figure 5: LB-positive large neurons contain less PLA signal than their neighbouring LB-negative neurons.
Large neurons (outlined in white in merged channels image) from DLB frontal cortex samples were manually selected based on DAPI-staining, and single-neuron PLA images were extracted and grouped into LB-positive (neuron 8) and LB-negative (neurons 1-7) neurons. Merged image displays PLA signal in red, pS129-positive LBs in grey, and nuclei in blue, while single-neuron images are shown in greyscale. LB-positive neurons contained significantly less PLA signal than neighbouring LB-negative neurons ($p=0.0451$). Groups were compared using a Wilcoxon matched pairs signed rank test, as they did not pass normality. Scale bar = 20 µm. n=28 images were analysed (containing a total of 30 LB-positive neurons and 114 LB-negative large neurons). Data are displayed as mean ± SEM of PLA particle area/image. * $p<0.05$.

Supplementary figure 6

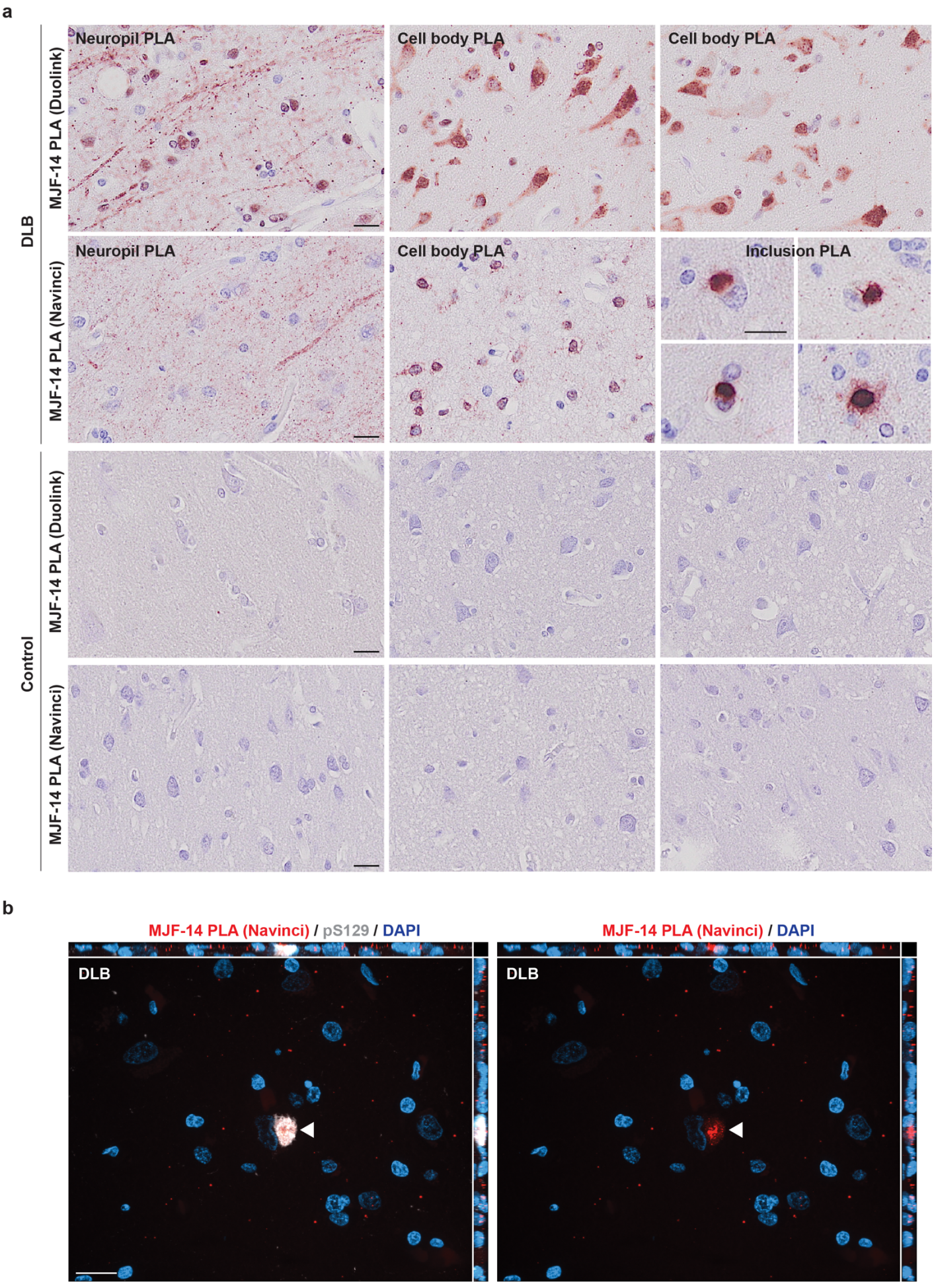

Supplementary figure 6: Validation stainings for Navinci MJF-14 PLA on DLB motor cortex.
a Chromogenic PLA overview of the motor cortex from DLB (top) and non-neurodegenerative control (bottom), stained with MJF-14 PLA from either Duolink or Navinci, exemplifying areas with preferential staining in the neuropil or the cell body. Note that strong labelling of inclusions is only seen with Navinci MJF-14 PLA. Scale bars = 20 µm. **b** Maximum intensity projection incl. orthogonal views of DLB motor cortex stained for Navinci MJF-14 PLA (red), serine-129 phosphorylated α-synuclein (pS129, grey), and DAPI nuclear stain (blue). Arrowhead indicates a pS129-labelled LB, which is also labelled by the Navinci MJF-14 PLA, in contrast to the Duolink MJF-14 PLA results in Fig. 3e. Scale bar = 20 µm.

Supplementary figure 7

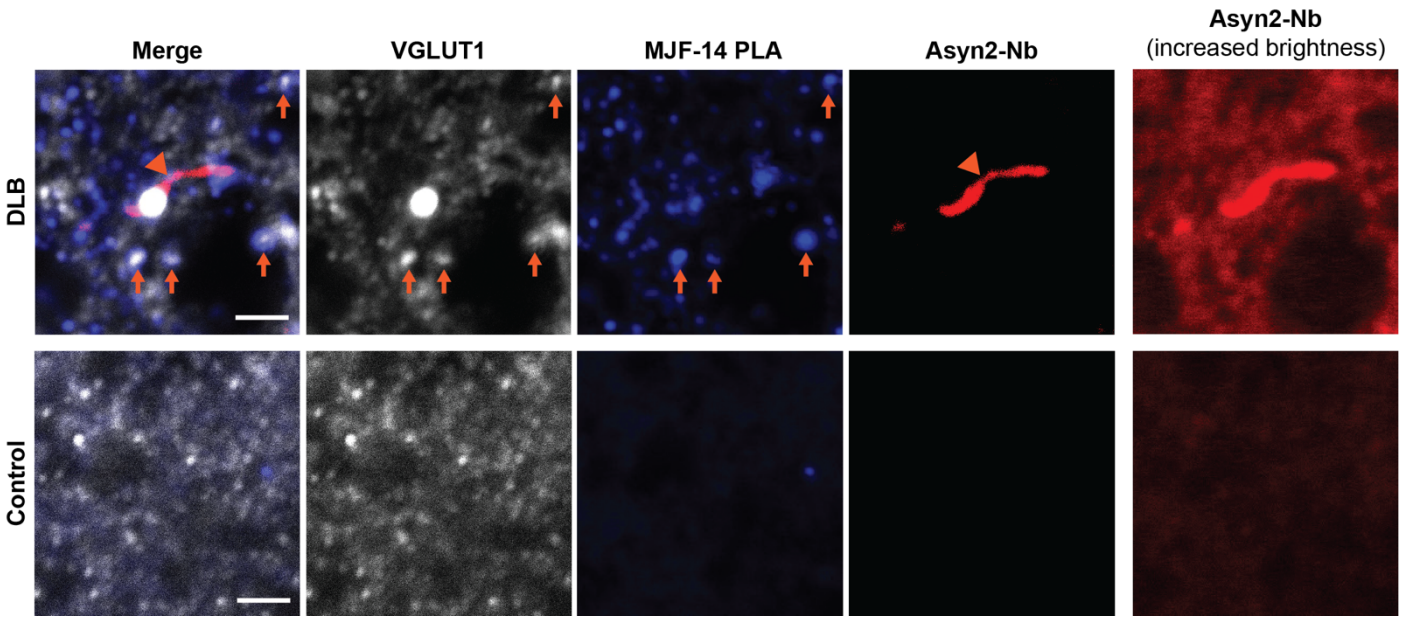

Supplementary figure 7: Non-expanded supplementary stainings for expansion PLA experiment.
Confocal images from non-expanded staining samples in the expansion PLA setup, with excitatory presynaptic terminals (VGLUT1, white), α-synuclein aggregate PLA (Navinci MJF-14 PLA, blue), and total α-synuclein (Asyn2-Nb, red). A Lewy neurite (most likely located in an axon) is stained by Asyn2-Nb (arrowhead), while examples of apparent PLA-VGLUT1 co-localization are indicated by arrows. An increased brightness version of the Asyn2-Nb channel is shown on the right. Scale bar = 2 µm.

Supplementary figure 8

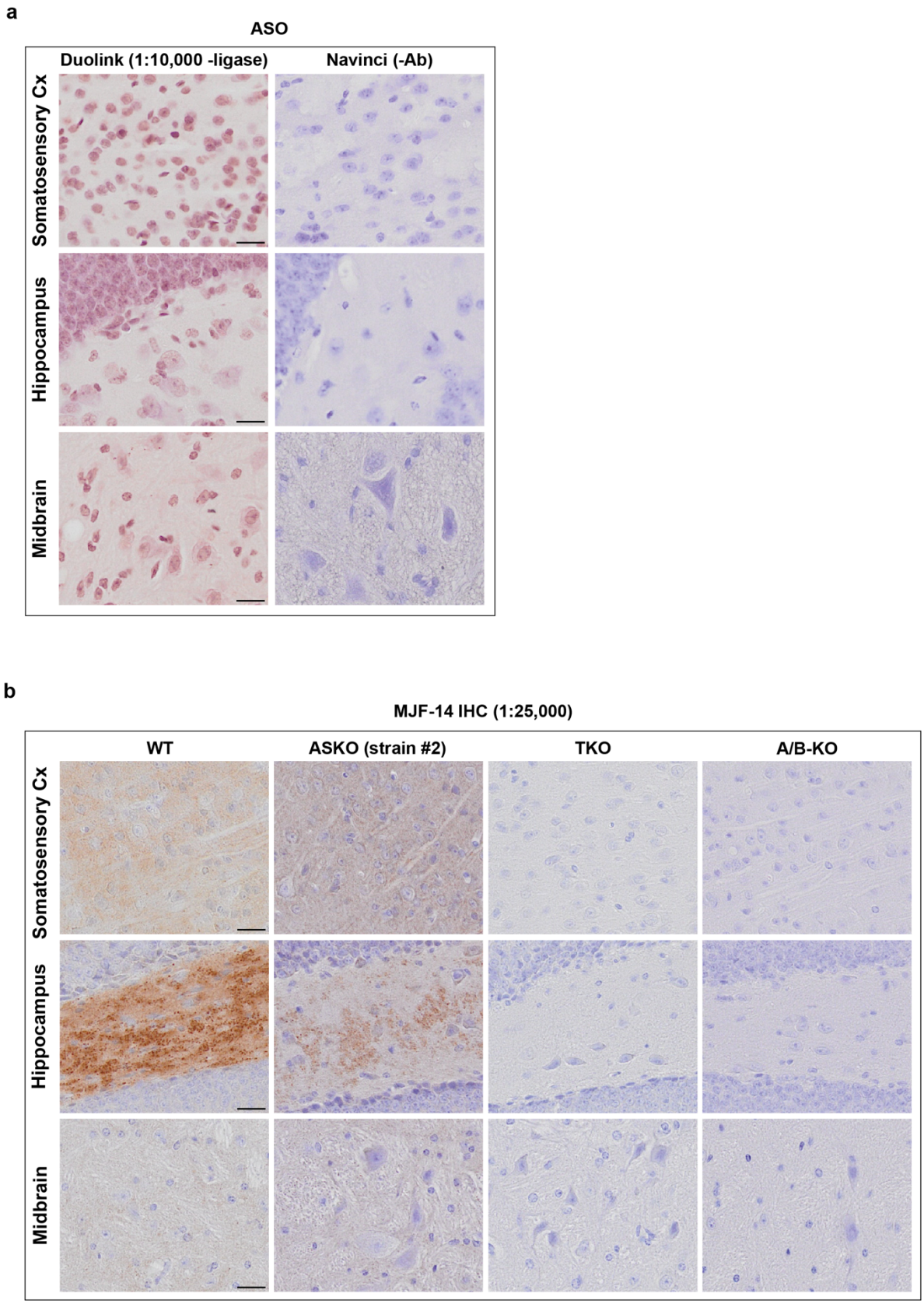

Supplementary figure 8: Technical negative PLA controls and IHC staining of mouse models.
a Technical negative control staining for MJF-14 PLA, lacking either the ligase in the PLA reaction (preventing signal formation) or the primary PLA antibody. The lack of signal in the controls demonstrate that insufficient blocking of endogenous peroxidase is not the cause for signal in ASKO mice. **b** MJF-14 IHC also shows signal presence in ASKO mouse tissue, confirming the issue to be antibody-related. As both α-/β-/γ-synuclein triple knockout and α-/β-KO mice are blank, cross-detection of β-synuclein is most likely the cause of the signal. Scale bars = 20 µm.

Supplementary figure 9

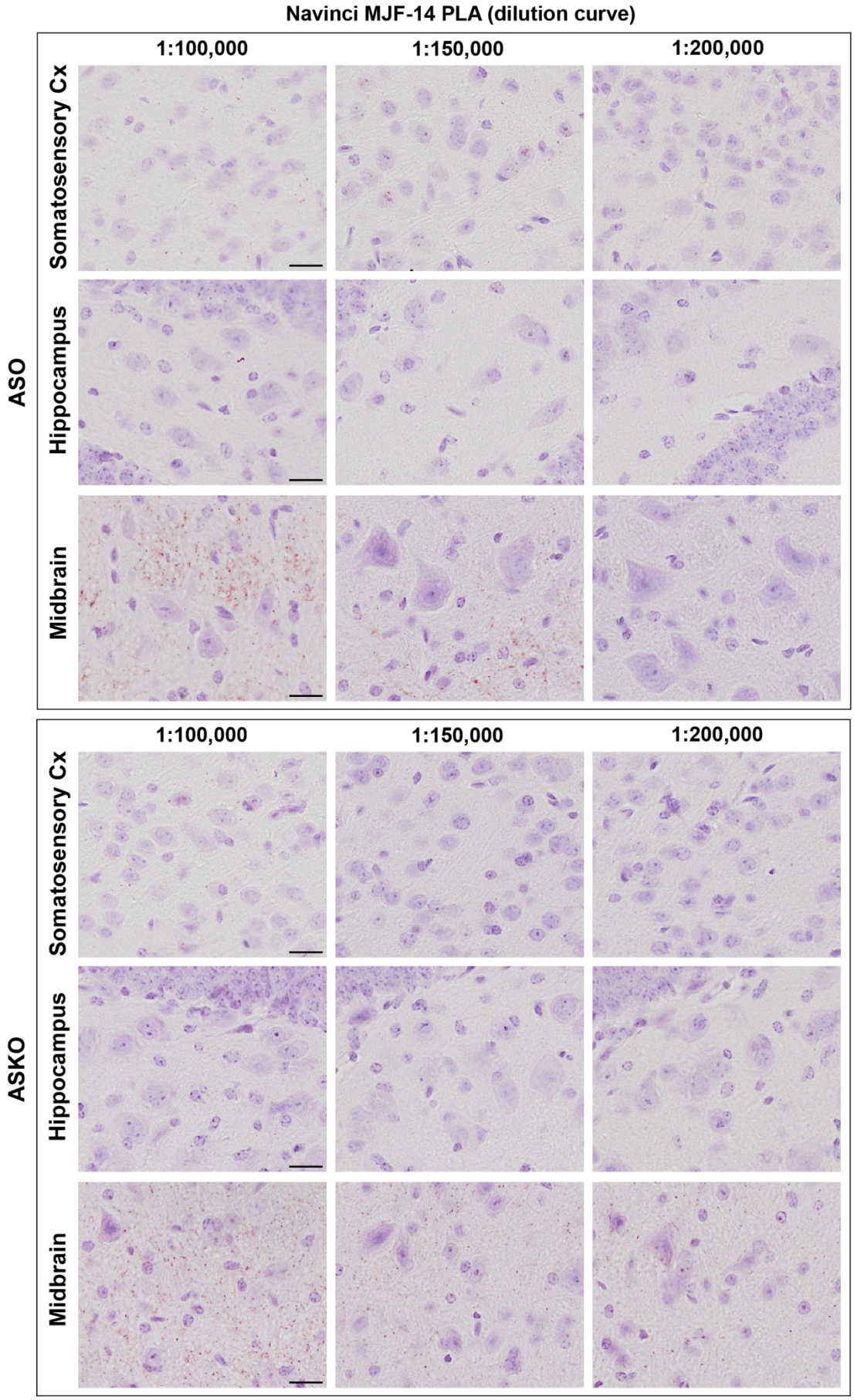

Supplementary figure 9: Dilution curve of Navinci MJF-14 PLA in mouse models.
Navinci MJF-14 PLA at dilutions up to 1:200,000 demonstrate that the antibody cannot be diluted further to abolish signal in the ASKO mice without simultaneously losing all signal in the ASO transgenic mice. Scale bars = 20 µm.

Supplementary tables

Supplementary Table 1 Demography of the DLB cases

	Sex	Age	Post-mortem delay (hours)	Disease duration (years)	Braak stage	Brain regions
DLB 1	Female	82	11	12	VI	Frontal cortex
DLB 2	Female	80	9.5	17	VI	Frontal cortex Motor cortex

Supplementary Table 2 Main cause of death in PD and control cases

Case number	Main cause of death
Control 1	Carcinoma of the lung
Control 2	Renal failure
Control 3	Myocardial infarction
Control 4	Ischaemic heart disease
Control 5	Renal failure
Control 6	Gastrointestinal tract bleeding
Control 7	Metastatic carcinoma
Control 8	Post-operation
Control 9	Sepsis
Control 10	Myocardial infarction
PD stage IV-1	Acute myocardial infarction
PD stage IV-2	Cardiopulmonary arrest
PD stage IV-3	Cardiorespiratory failure
PD stage IV-4	Ischaemic heart disease
PD stage IV-5	Cerebrovascular event
PD stage IV-6	Pneumonia
PD stage IV-7	Pneumonia
PD stage IV-8	Dehydration
PD stage IV-9	Pneumonia
PD stage IV-10	Ischaemic heart disease
PD stage VI-1	Cerebrovascular event
PD stage VI-2	Carcinoma of the prostate
PD stage VI-3	Renal failure, acute myocardial infarction
PD stage VI-4	Pulmonary embolism
PD stage VI-5	Pneumonia
PD stage VI-6	Senile dementia
PD stage VI-7	Cardiorespiratory arrest
PD stage VI-8	Cerebrovascular accident
PD stage VI-9	End-stage Parkinson’s disease
PD stage VI-10	End-stage Parkinson’s disease

Supplementary Table 3 PLA particles/case and division of cases by counterstain efficiency

Section no.	Category	ACC region	Group 1: Intense counterstain	Group 2: Weak counterstain	PLA particles/image
1	Control	DGM		X	15
		SGM		X	4
2	PD stage IV	DGM		X	349
		SGM		X	377
3	PD stage VI	DGM		X	366
		SGM		X	212
8	PD stage VI	DGM	X		896
		SGM	X		1413
9	PD stage IV	DGM	X		574
		SGM	X		737
10	Control	DGM		X	3
		SGM		X	3
11	Control	DGM		X	17
		SGM		X	15
12	PD stage IV	DGM		X	446
		SGM		X	64
13	PD stage VI	DGM		X	105
		SGM		X	52
18	PD stage IV	DGM		X	187
		SGM		X	237
19	PD stage VI	DGM	X		736
		SGM	X		958
20	Control	DGM		X	21
		SGM		X	34
21	Control	DGM		X	5
		SGM		X	10
22	PD stage IV	DGM	X		112
		SGM	X		192
23	PD stage VI	DGM	X		60
		SGM	X		28
28	PD stage VI	DGM		X	60
		SGM		X	110
29	PD stage IV	DGM	X		1049
		SGM	X		1093
30	Control	DGM	X		5
		SGM	X		22
31	Control	DGM		X	37
		SGM		X	13
32	PD stage IV	DGM		X	1031
		SGM		X	1109
33	PD stage VI	DGM		X	949
		SGM		X	2771
38	PD stage VI	DGM		X	933
		SGM		X	1389
39	PD stage IV	DGM		X	1264
		SGM		X	881
40	Control	DGM		X	4
		SGM		X	6
41	Control	DGM		X	8
		SGM		X	18
42	PD stage IV	DGM	X		441
		SGM	X		377
43	PD stage VI	DGM	X		1006
		SGM	X		895
48	PD stage VI	DGM		X	344
		SGM		X	1092
49	PD stage IV	DGM	X		570
		SGM	X		536
50	Control	DGM	X		238
		SGM	X		62

Supplementary Table 4 Comparison of the signal density of PLA and IHC (data presented as mean ± SEM)

	Controls	PD stage IV	PD stage VI
Total PLA/mm^2	140.28±466.41	2766.61±464.53***	3178.48±494.15***
Total deposit particles/mm^2	2.91±5.81	16.75±5.79	39.20±6.03***$^{\#}$
Total LBs/mm^2	0.11±1.81	3.62±1.80	14.47±1.87***$^{\#\#\#}$

Univariate tests with covarying age, sex, PMD. Compared to control, *** p<0.001. Compared to stage IV PD, $^{\#}$ p<0.05, $^{\#\#\#}$ p<0.001.

Supplementary Table 5 Neuronal signal density of PLA and IHC (data presented as mean ± SEM)

	Controls	PD stage IV	PD stage VI
PLA particle containing neurons (%)	6.76±5.54	70.50±5.52***	63.51±5.75***
Deposit particle containing neurons (%)	0.50±1.90	4.70±1.80	10.70±1.90***$^{\#}$
LB containing neurons (%)	0.00±0.59	0.87±0.58	4.13±0.61***$^{\#\#\#}$

Univariate tests with covarying age, sex, PMD. Compared to control, *** p<0.001. Compared to stage IV PD, $^{\#}$ p<0.05, $^{\#\#\#}$ p<0.001.

The covariate value in the LB containing neurons of control was rounded to 0.00.

Supplementary Table 6 Average PLA particle count in affected neurons (data presented as mean ± SEM)

	Controls	PD stage IV	PD stage VI
Superficial grey matter (SGM)	1.09±0.58	2.09±0.54	3.40±0.60*
Deep grey matter (DGM)	1.12±0.29	2.23±0.24**	2.18±0.26*

Univariate tests with covarying age, sex, PMD. Compared to control, * p<0.05, ** p<0.01.

Supplementary Table 7 Neuronal, extracellular, and glial density of PLA signals in controls versus PD (data presented as mean ± SEM)

	Category criteria	Controls	PD stage IV	PD stage VI
Proportion of neuronal nuclear type in total neurons (%)	With ≥ one particle in the neuronal nucleus	1.67±1.20	6.23±1.08**	5.44±1.11*
Proportion of cytoplasmic type in total neurons (%)	With ≥ one particle in the neuronal cytoplasm	6.64±3.98	41.08±3.58***	30.83±3.68***
Proportion of mixed type in total neurons (%)	With ≥ one particle in the neuronal nucleus and cytoplasm	0.28±4.84	23.44±4.36***	27.14±4.48***
Proportion of PLA particle containing neurons (%)		6.76±5.54	70.50±5.52***	63.51±5.75***
Extracellular & glial PLA/mm^2		63.10±336.93	1778.30±335.57***	2336.68±349.74***
Proportion of total PLA particles located in neuronal nuclei & cytoplasm (%)		35.81±8.14	33.63±4.62	28.92±2.96
Proportion of total PLA particles located in neuropil/extracellular/glial space (%)		64.19±8.14	66.37±4.62	71.08±2.96

Univariate tests with covarying age, sex, PMD. Compared to control, * p<0.05, ** p<0.01, *** p<0.001.